PAPER

Plasma interaction with emmissive surface with Debye-scale grooves

IOP Publishing Plasma Sources Science and Technology
Plasma Sources Sci. Technol. 27 (2018) 045004 (6pp) https://doi.org/10.1088/1361-6595/aab6d8

Plasma interaction with emmissive surface with Debye-scale grooves

Irina Schweigert[1,2,5], Thomas S Burton[3], Gregory B Thompson[3], Samuel Langendorf[4], Mitchell L R Walker[4] and Michael Keidar[1]

[1] George Washington University, Washington, DC 20052, United States of America
[2] Khristianovich Institute of Theoretical and Applied Mechanics, Novosibirsk 630090, Russia
[3] The University of Alabama, Tuscaloosa, AL, 35487, United States of America
[4] Georgia Institute of Technology, Atlanta, GA, 30332, United States of America

E-mail: ischweig@yahoo.com

Received 28 November 2017, revised 2 March 2018
Accepted for publication 15 March 2018
Published 5 April 2018

Abstract

The sheath development over emissive grooved surface in dc discharge plasma controlled by an electron beam is studied in the experiment and in 2D kinetic simulations. Grooved hexagonal boron nitride surfaces with different aspect ratios, designed to mimic the erosion channels, were exposed to an argon plasma. The characteristic size of the grooves (1 mm and 5 mm) is about of the Debye length. The secondary electrons emission from the grooved surfaces is provided by the bombardment with energetic electrons originated from the heated powered cathode. The transition between a developed and a collapsed sheaths near emissive surface takes place with an increase of the beam electron energy. For grooved emissive surfaces, the sheath transition happens at essentially higher voltage compared to the planar one. This phenomenon is analyzed in the terms of the electron energy distribution function.

Keywords: plasma-wall interaction, grooved surface, secondary electron emission, sheath transition, discharge plasma

1. Introduction

The surface wall morphology in plasma devices can evolve with time due to a dynamic plasma-wall interaction that leads to drastic change of all plasma characteristics. For example, in Hall effect thrusters, plasma–wall interactions have been found to play a key role in the thruster operation and performance [1–5]. In [2], radially symmetric surface modulations, at a larger characteristic length scale than the plasma sheath thickness were observed in the discharge plasma for an extensive time operation. Sub- and near sub-micron erosion patterns in a hexagonal boron nitride (hBN)—amorphous silica Hall effect thruster's wall material exposed to a krypton plasma were found in [6]. Using different metallographically polished hBN surface finishes, the influence of roughness on plasma sheath potential was observed in [7]. In the cases of smooth or rough surfaces, the secondary electron emission (SEE) yield from the wall can be different, and can affects the plasma sheath structure. Effects of surface features smaller-than-Debye length scales on SEE were previously found to be consistent with a trapping of the secondary electrons near the wall surface [8]. For much higher gas pressure in [9], the magnitude of the sheath electric field above a grooved electrode was measured in a parallel-plate RF discharge for the case when the sheath thickness is on the same order as the surface features. It was shown that due to the significant electric field modulation above the grooves the ion trajectories were strongly deflected.

Though the alterations of the wall surface in plasma devices can take many hours of operation, quantifying the effect of the complex surface topology on the plasma sheath is important for predicting device efficiency and long term behavior. The transition in sheath structure near the planar emissive surface is studied quite intensively since original work of Hobbs and Wesson [10]. The subject of this study is the plasma interaction with the emissive surface with a Debye length scale grooved topology. In the experiment and in 2D3V particle-in-cell Monte Carlo collision (PIC MCC) simulations, we study the effect of the SEE from the floating grooved plate on plasma sheath at low gas pressure. The discharge operation and SEE from the hBN plate are controlled by an electron beam from heated cathode. A change in

[5] Author to whom any correspondence should be addressed.

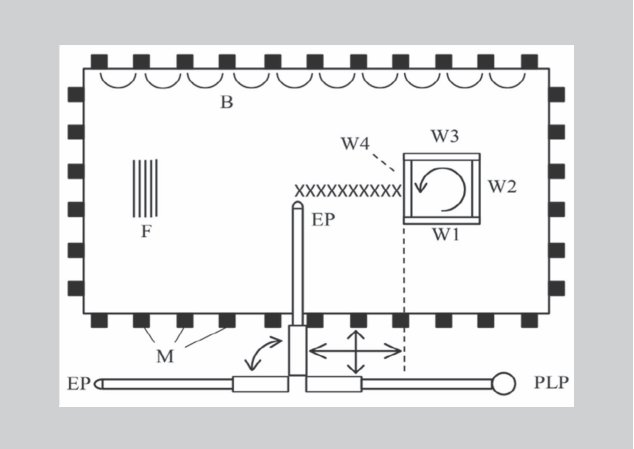

Figure 1. Diagram of plasma cell and diagnostics. F = filaments, M = magnets, B = nominal magnetic field, PLP = planar Langmuir probe, EP = emissive probe, W = wall material sample. Emissive probe orientation rotated 90° in figure to show hairpin tip geometry. Not to scale.

the energy of beam electrons initiates the transition between different types of the wall sheath near a emissive floating plate with (a) planar and (b) grooved surfaces.

This paper is organized as follows. The experimental setup, wall material samples and diagnostics are described in section 2. The kinetic model of discharge plasma with an electron beam and emissive grooved surface is given in section 3. PIC MCC simulation results on the transition between different sheath types near the emissive surface and a comparison with experimental data are presented in section 4. In section 5, the conclusions are given.

2. Experimental setup

2.1. Plasma device

The plasma was generated in a low-density multi-dipole plasma cell lined with permanent magnets that created confining cusp fields, as shown in figure 1. These cusp magnetic fields decay rapidly away from the permanent magnet dipoles around the boundary, so the main plasma volume of the device is not magnetized. The cell was cylindrical in shape and had a radius of 30.5 cm and a height of 91 cm with the cell walls being aluminum and grounded. Typical plasma density used was approximately 10^7 cm^{-3} and with 1%–10% of the energetic electrons population.

The cathode is thoriated-tungsten filaments (F in figure 1). The voltage applied to the cathode ranges from −60 to −200 V. The thermoemission from filaments provides electrons, which are accelerated crossing the cathode sheath in the direction of the wall material sample (W in figure 1). These electrons form almost a monoenergetic beam with the energy corresponding to the cathode sheath potential drop which is approximately equal to the applied voltage U.

The plasma cell was housed in a large vacuum chamber which achieved a base pressure of 10^{-8} Torr. During operation, 500 sccm of argon was flowed into the chamber using a MKS 1179A01352CS1BV mass flow controller to achieve the experimental pressure of $P = 10^{-4}$ Torr.

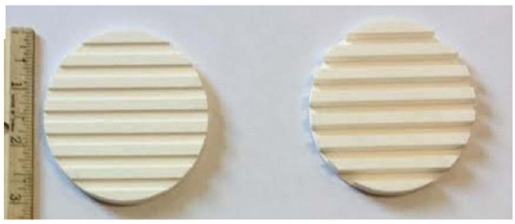

Figure 2. hBN disks with machined grooves with depth of 1 mm (left) and 5 mm (right).

2.2. Wall material samples

Disks made from hBN material were 7.6 cm in diameter and 0.64 cm in thickness. This material has a large SEE yield which increases with the energy of incident electrons. It is also a commonly used ceramic wall material in Hall effect thrustes. The 5 mm wide grooves were machined into the surface of the disks shown in figure 2, which were spaced 10 mm apart with uniform depths of either 1 or 5 mm. A control disk with no grooves was also used for comparison. Prior to insertion into the plasma chamber, the disks were cleaned with acetone, deionized water then air dried. The hBN disks were mounted to a box holder made of stainless steel.

2.3. Diagnostics

In the experiment, the bulk plasma parameters are measured with a tungsten planar-disc Langmuir probe. A linear portion of the current–voltage (I–V) characteristic is observed at biases above the cathode potential and below the plasma potential due to the isoptropic and largely monoenergetic electron population accelerated from the emissive filament cathode. This region fits well with the theory of Hershkowitz *et al* [11], and is analyzed according to that theory to determine the energetic electron number density $n_{\rm be}$ with the formula from [11]

$$n_{\rm be} = -\frac{{\rm d}I}{{\rm d}V}\frac{2m_e v_{\rm be}}{e^2 S},$$

where V is the probe bias voltage and S is the Langmuir probe surface. Colder Maxwellian electron populations are also observed. The Debye length is calculated including the contribution of all measured electron populations, and is found to be in the range of 3–5 mm for $U = -60$ to -200 V.

The sheath potential over the wall material samples was measured using an emissive probe constructed of telescoping alumina tubing and a hairpin 0.127 mm diameter thoriated tungsten filament tip. The emissive probe is biased with a Keithley 2410 Sourcemeter. Bulk plasma parameters were measured using a planar Langmuir probe positioned in the center of the plasma device. The probe was cleaned by ion bombardment at −500 V bias for a period of 15 min before data collection; the probe was re-cleaned at −500 V for 30 s after the collection of each trace. The Langmuir probe body was constructed of alumina tubing. The tip was made from

0.5 mm thick tungsten foil. Five linear stair sweeps from −200 to 0 V were collected with an average dwell time of 20 ms at each voltage at a step interval of 0.2V. The probe characteristics were corrected for singly charged argon ion- and electron-induced SEE using data for tungsten from [12].

3. Theoretical model and malculation details

To understand the mechanism of sheath formation over the surface with a complex topology in discharge plasma we use the model from [13] developed for the planar surface case. The discharge plasma and the sheath near the planar or grooved floating emissive plates are simulated for our experimental conditions with 2D3V PIC MCC method.

The Boltzmann equations are solved to find the distribution functions for electrons $f_e(\vec{r}, \vec{v})$ and ions $f_i(\vec{r}, \vec{v})$

$$\frac{\partial f_e}{\partial t} + \vec{v}_e \frac{\partial f_e}{\partial \vec{r}} - \frac{e\vec{E}}{m}\frac{\partial f_e}{\partial \vec{v}_e} = J_e, \quad n_e = \int f_e \, \mathrm{d}\vec{v}_e, \tag{1}$$

$$\frac{\partial f_i}{\partial t} + \vec{v}_i \frac{\partial f_i}{\partial \vec{r}} + \frac{e\vec{E}}{M}\frac{\partial f_i}{\partial \vec{v}_i} = J_i, \quad n_i = \int f_i \, \mathrm{d}\vec{v}_i, \tag{2}$$

where v_e, v_i, n_e, n_i, m, M are the electron and ion velocities, densities and masses, respectively. The collisional integral for electrons J_e includes the elastic scattering, excitation and ionization [14, 15] in argon gas. For ions, the collisional integral J_i includes the resonance charge exchange collisions with background argon gas.

The Poisson equation describes the electrical potential and electrical field distributions

$$\triangle\phi = 4\pi e(n_e - n_i), \quad \vec{E} = -\frac{\partial \phi}{\partial \vec{r}}. \tag{3}$$

In simulations, the calculation domain is 13 cm over z-axis, 8 cm over x-axis and $x = 0$ is the axis of symmetry. The cathode of 3.2 cm over x is placed 0.5 cm above the bottom of the chamber. The periodic boundary conditions are set the right boundary of calculation domain at $x = 8$ cm for electron and ion transport in x-direction. For the Poisson equation the boundary conditions are $\phi = U$ at the cathode, $\phi = 0$ at $z = 0$ and $z = 13$ cm, the electrical field $E_x = 0$ at $x = 8$ cm. The grid for calculation is non-uniform with the number of nodes $N_z = 200$ and $N_x = 150$. The grid over z is thickened at the cathode and at the grooved surface. At $z > 10$ cm the grid is uniform over z (starting at 1 cm from grooved surface and inside of grooves) with step $\Delta z = 0.025$ cm (120 nodes). Over axis x, the grid is uniform with step $\Delta x = 0.025$ cm at $x < 3$ cm (120 nodes) and Δx increases in the direction to the right boundary of the calculation domain. The time step is $\Delta t = 0.5 \times 10^{-12}$ s. The number of psudo particles for every type of species is approximately (1–2) $\times 10^6$.

Since the BN-plate is under the floating potential the total current on it $j_{\text{total}} = 0$. In PIC MCC simulations, to find this floating potential we (a) calculate electron and ion fluxes to the BN-plate on every electron time step and if the total flux is not zero within 5% of statistical error, then (b) the potential of the BN-plate surface is corrected to provide a zero-current condition. As a result, the potential and the field distributions in plasma and on the BN-plate surface reach a steady-state which depends on the energy of electron beam. This floating potential of BN-plate surface is the boundary condition for the electric potential. In figure 3, a part of calculation domain with the grooves of 5 mm wide and 5 mm depth is shown. In simulations, the wall material sample has four identical trenches, but in figure 3, there are only two grooves shown, since $x = 0$ is the axis of symmetry. For grooved plate, the floating potential is calculated separately for four different surface fragments shown in figure 3: for left (1) and right (2) sides of trenches, for front surface (3) and for trench bottom (4).

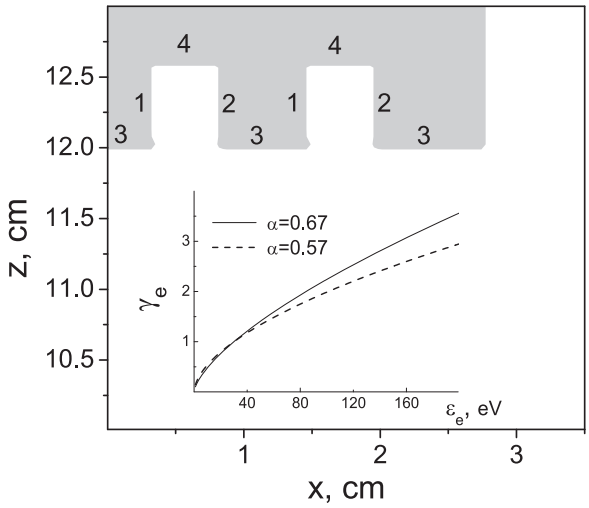

Figure 3. Grooves geometry in simulation. 1, 2, 3, 4 refer to different fragments of grooves for separate calculation of floating potential. Insert shows secondary electron emission coefficient for hBN as function of electron energy.

The beam electrons are emitted from the cathode surface and accelerated within the cathode sheath to the direction of grooved plate. In simulations, we took a SEE coefficient γ_{see} in the form $\gamma_{\text{see}} = (\epsilon_e/E)^\alpha$, where $E = 30$ and $\alpha = 0.67$ (see figure 3, insert). The SEE coefficient from [16], $\gamma_{\text{see}} = (\epsilon_e/E)^\alpha$ with $E = 30$ and $\alpha = 0.57$ is also given in figure 3. In the simulation, a larger α is taken to obtain a better agreement with our experimental observations. In the experiment, the sheath transition for a 5 mm grooved plate was observed at $U = -175$ V. In the simulation with smaller $\alpha = 0.57$, the transition happens at $U = -205$ V and with $\alpha = 0.67$ in a range from −175 to −190 V.

The cathode voltage U ranges from −70 to −200 V, the gas pressure is 10^{-4} Torr. The system of equations (1)–(3) is written in the Cartesian coordinates and solved with PlasmaNOV code (see for details [17]).

4. 2D3V PIC simulation results

In simulations and in the experiment, the volume ionization, as well as the secondary emission from the BN-plate are sustained by a beam of energetic electrons. In simulations, the

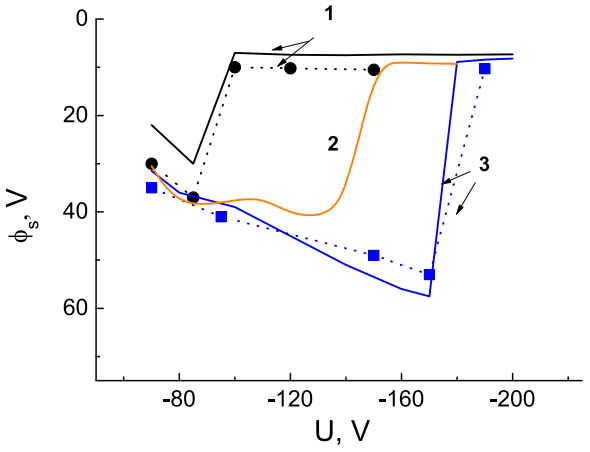

Figure 4. Potential drop near BN-plate as function of applied voltage for planar (1) and grooved surfaces with depth of 1 mm (2) and 5 mm (3). Experimental data (solid lines) and calculations (symbols).

number of energetic electrons was taken from the experimental data. The initial velocities of the electron from the filaments is a half Maxwellian distribution with the mean electron temperature $T_e = 1$ eV. With changing applied voltage U from -70 to -200 V, the energy of beam electrons rises almost from 70 to 200 eV. It leads to an increase of the number of secondary electrons emitted from the surface, since $\gamma(\epsilon_e)$ is a growing function of the electron energy.

A monotonic increase of U eventually results in a collapse of the sheath near BN-plate. Both measured and calculated data shown in figure 4 exhibit a rapid transition from developed to collapsed sheath types at some critical voltage U_{cr}. The potential drop $\Delta\phi$ over the sheath diminishes approximately in 3–5 times for planar and grooved plates during transition, but it happens at different voltages. For the planar plate, the transition happens at $U_{cr} = -90$ V, for the 0.1 cm grooves case $U_{cr} = -140$ V and for the 0.5 cm grooves case $U_{cr} = -175$ V. Note that for grooves with $l = 0.5$ cm the critical voltage is approximately twice larger compared to the planar plate one. As seen in figure 4, a decrease of grooves characteristic size causes a lowering the critical voltage and in the limit of $l \ll \lambda_D$, the sheath development will not depend on surface topology. More complex processes take place for the case of larger grooves with $l \gg \lambda_D$, when sheaths form inside of the trenches and the dynamics of electron heating essentially changes (see for example [18]).

The calculated and measured electron density n_e and the electron temperature T_e before and after the transition are shown in figure 5 for grooved surface for $U = -70$ and -190 V. In the experiment, the n_e and T_e were measured 3 and 5 cm apart from the emissive surface for $U = -70$ V. It is seen that after transition the density of plasma decreases by factor of 2 and the mean temperature rises. The density of electrons increases near the surface due to accumulation of emitted low energy secondary electrons. The calculated and measured electron temperature is averaged over all groups of electrons.

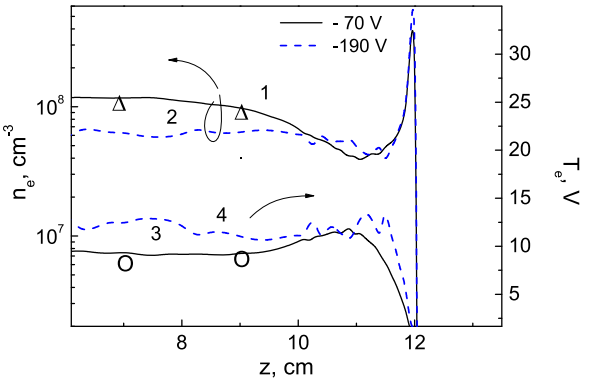

Figure 5. Electron density and temperature distributions over axis of symmetry for $U = -70$ V (1, 3) and -190 V (2, 4) for grooved surface. Symbols are the experimental data measured 3 cm and 5 cm apart from the grooved surface for $U = -70$ V.

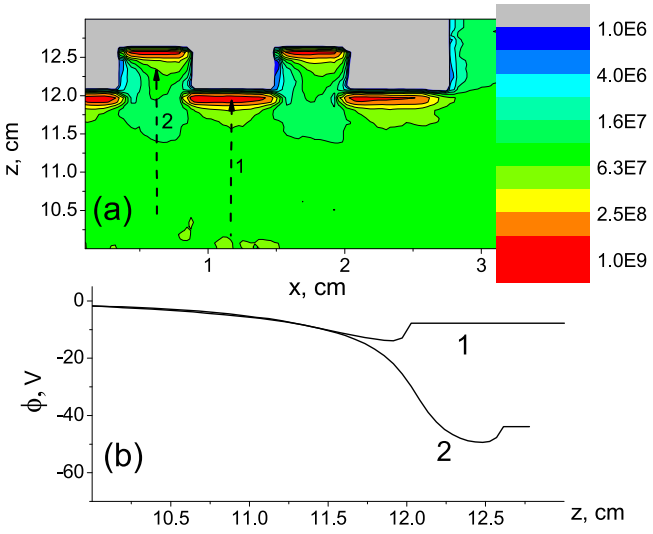

Figure 6. Electron density distributions for grooved surface (a) and potential profiles (b) along arrows 1 and 2 shown in (a) for $U = -190$ V.

For all our experimental conditions $T_e = 8$–12 eV and the n_e is in a range of (5–10) $\times$ 10^7 cm^{-3} in quasineutral plasma and (1–5) $\times$ 10^7 cm^{-3} within the sheath over the emissive plate. The Debye length, λ_D (cm) $= 742 \times (T_e/n_e)^{0.5}$, ($T_e$ in eV and n_e in cm^{-3}), varies from 0.25 cm to 0.5 cm for our plasma parameters. The wall material samples in our study are grooved with a trench size $l \approx \lambda_D$ and the sheath could not form inside of the grooves.

An example of spatial distribution of electron density is shown in figure 6(a) for applied voltage $U = -190$ V. The peaks of density of low energy secondary electrons and associated with them virtual cathodes arise near the emissive surface. In figure 6(b), the potential distribution is given along the arrows (1) and (2) shown in figure 6(a). The virtual cathode looks as a dip in the potential profile near the emissive surface exposed by the energetic electrons. In this case, in quasineutral plasma the densities of beam energetic electrons and the low energy electrons are $n_{be} = 0.26 \times 10^7$ cm^{-3} and $n_{pe} = 5.2 \times 10^7$ cm^{-3}, respectively.

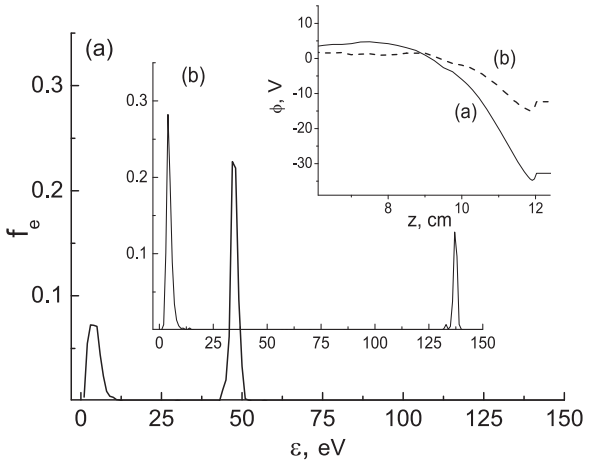

Figure 7. Energy distribution function of electrons approaching planar surface at $U = -85$ V (a) and -150 V (b). Insert: potential profiles over z at $x = 0$ for $U = -85$ V (a) and -150 V (b).

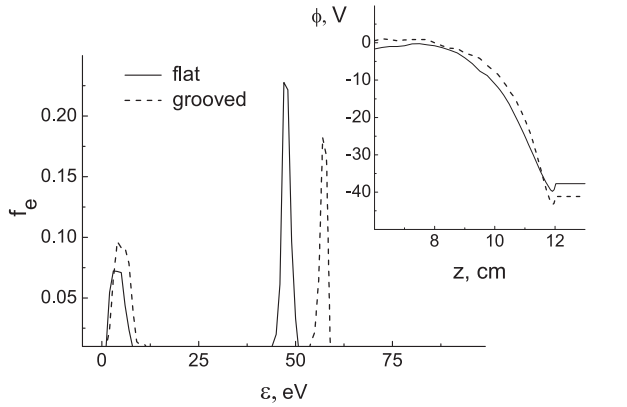

Figure 8. Electron distribution function for electrons approaching the front surface of planar (solid line) and grooved (dashed line) plates for $U = -85$ V and -95 V, respectively. In insert: potential profiles over z at $x = 0$ for planar (solid line) and grooved surfaces (dashed line).

Let us consider the mechanism responsible for a delay of the sheath transition near the grooved emissive surface compared to the control planar plate. For our experimental conditions the sheath near emissive surface forms depending on a contribution of secondary electrons even for smaller applied voltage. The sheath is not a Debye type, and the ion current to the surface is negligible. The zero-current condition to the surface under floating potential is

$$j_{pe} + j_{esr} + j_{be} = j_{be} \times \gamma(\epsilon_e), \tag{4}$$

where j_{pe} is the current of low energy plasma electrons, j_{esr} is the current of secondary electrons, scattered back to the surface and j_{be} is the current of beam electrons from plasma. During the transition the sheath near BN-plate collapses to allow the low energy electrons to cross the sheath and enlarge the electron current to the emissive surface.

The question why the critical voltage increases for complex topology with Debye scale grooves can be answered on the basis of analysis of the electron energy distribution function (EEDF) and potential distribution over the surface. Let us first consider the EEDF modification with U for the planar surface. In figure 7, the EDF of electrons approaching the surface and the potential profiles before and after transition are shown over the planar surface at $U = -85$ V and $U = -150$ V. The spectra of electrons approaching the surface have two peaks corresponding to low energy electrons from bulk plasma and the energetic of beam electrons. A lower energy peak includes also the secondary electrons scattered back to the plate from the virtual cathode. As seen in figure 7 (insert), the virtual cathode with a 3.5 V depth occurs before and after transition. Since the sheath potential drop $\Delta\phi$ diminishes from 40 to 10 V during transition, the EEDF has larger population of low energy electrons for $U = -150$ V after transition. The energy of beam electrons is $\epsilon_{be} = e(U - \Delta\phi)$. As seen in figure 7, for $U = -85$ V, $\Delta\phi = 33$ V and the beam electron energy equals to 53 eV. For the case of $U = -150$ V, $\epsilon_{be} = 137$ eV.

To understand why the critical voltage is larger for grooved surface let us compare the EEDFs for different

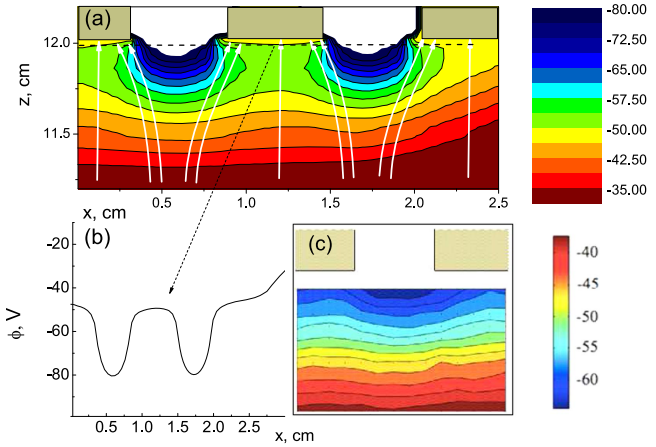

Figure 9. Electrical potential distribution calculated (a), (b) and measured (c) for $U = -150$ V. The color map for (c) is from -35 V up to -70 V. White arrows show schematically the electron trajectories. (b) Presents the potential profile along dashed line shown in (a).

surface topology. In figure 8, EDFs of electrons approaching the planar surface at $U = -85$ V and grooved one at $U = -95$ V are shown. For the grooved surface, the calculated EDF includes the electrons arriving to the front surface (3 in figure 3). For both cases, the sheath potential drop $\Delta\phi \approx 40$ V. For the planar surface, $U = -85$ V is the case just before transition, but for the grooved surface the case of $U = -95$ V is still far away from the transition point. As seen in figure 8, for both cases the EEDF has two groups of electrons, but for grooved surface the population of group of low energy plasma electrons is larger. This is a key finding which explains the enlarged U_{cr} for grooved surface.

An enrichment of the group of low energy electrons is provided with a deflection of the flux of low energy electrons from the orifice of grooves to the front surface. This focusing effect is due to a non-monotonic potential distribution along grooved surface. Note, that the flux of energetic beam electrons is weakly disturbed by the electrical field E_x and it

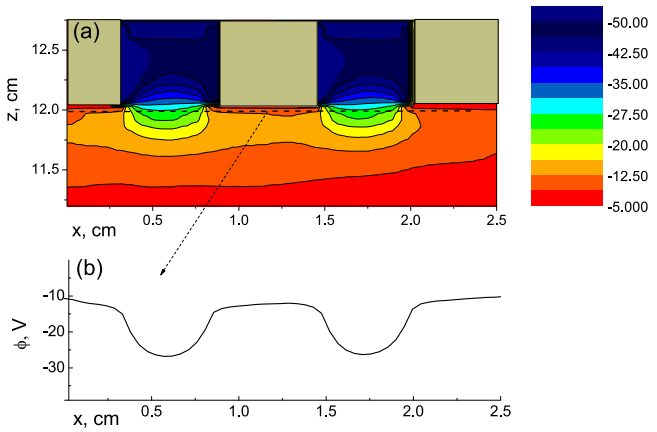

Figure 10. Calculated electrical potential for $U = -190$ V. (b) The potential profile along dashed line shown in (a).

penetrates inside of grooves. In figure 9, PIC MCC simulation results and experimental data on the potential distribution are shown for $U = -150$ V. Both computed and measured results demonstrate the non-monotonic potential distribution with a strong gradient over x along the grooved surface. In figure 9(a), the white arrows schematically present the trajectories of low energy electrons. Figure 9(b) shows the electrical potential profile along the dashed line given in figure 9(a). The measurements in figure 9(c) were done with steps of 1 mm over the grooves surface and of 0.5 mm in normal direction. The domain of measurement of 13 mm over x and 6 mm over z is 1 mm apart from the surface. The electrical potential distribution acts as a focusing lens on the low energy electrons current and redirect them to the front surface. Note that these additional low energy electrons do not produce the secondary electrons from the surface. In another words, in left hand of equation (4), the current j_{pe} increases approximately by factor of 2, therefore the critical voltage increases for the grooved case.

The calculated potential distribution after transition is shown in figure 10 for $U = -190$ V. It is seen that for the grooved surface, the transition takes place only near the front sheath. The $\Delta\phi$ drops from 48 to 10 V. Inside of trenches the potential drop remains large and only the beam electrons can overpass it.

5. Conclusion

The transition between different types of sheath near the emissive surface with Debye length grooves in low pressure plasma have been studied in the experiment and PIC MCC simulations. The ionization in the plasma volume and the SEE from grooved plate are set by the beam electrons initiated from biased filaments. The hBN disks with machined grooves with 1 mm and 5 mm depth on the surface were maintained in the plasma chamber to study the plasma interaction with emissive surface with a complex topology. These grooves mimic different degrees of erosion on the wall in plasma. With increasing voltage, the measured and calculated potential distributions over the BN-plate exhibit transition between different types of sheathes. This transition has been found to take place at a higher applied voltage for the surface with larger grooves. For 5 mm grooves depth, the critical voltage is almost two time higher as compared to the control planar surface case. An analysis of the energy distribution function of electrons arriving on the surface and the potential distribution gives us an explanation of this phenomenon. In the case of grooved surface, a non-monotonic potential distribution along the grooves is able to deflect the flux of low energy electron from the orifice of grooves to the front surface, whereas the flux of beam electrons remains practically undisturbed. The electric field component parallel to the surface is not strong enough to affect the beam electron current.

Acknowledgments

The authors gratefully acknowledge FA9550-11-1-0160, Program Manager Mitat Birkan for support of this research. One of authors, IS, was partly supported by RSF 17-19-01375.

ORCID iDs

Irina Schweigert https://orcid.org/0000-0002-2364-1228

References

[1] Keidar M, Boyd I D and Beilis I I 2001 *Phys. Plasmas* **8** 5315
[2] De Grys K, Mathers A, Welander B and Khayms V 2010 *46th AIAA /ASME/SAE/ASEE Joint Propulsion Conf. and Exhibit* AIAA 2010-6698
[3] Gascon N, Dudeck M and Barral S 2003 *Phys. Plasmas* **10** 4123
[4] Barral S, Makowski K, Peradzynski Z, Gascon N and Dudeck M 2003 *Phys. Plasmas* **10** 4137
[5] Hofer R R, Mikellides I G, Katz I and Goebel D M 2007 *30th Int. Electric Propulsion Conf., IEPC-2007-267* p 17
[6] Burton T, Schinder A M, Capuano G, Rimoli J J, Walker M L and Thompson G B J 2014 *Propulsion Power* **30** 690
[7] Langendorf S and Walker M 2015 *Phys. Plasmas* **22** 033515
[8] Raitses Y, Staack D, Dunaevsky A and Fisch N 2006 *J. Appl. Phys.* **99** 361031
[9] Czarnetzki U, Hebner G A, Luggenholscher D, Dobele H F and Riley M E 1999 *IEEE Trans. Plasma Sci.* **27** 70
[10] Hobbs G D and Wesson J A 1967 *Plasma Phys.* **9** 85
[11] Hershkowitz N, DeKock J R, Coakley P and Cartier S L 1980 *Rev. Sci. Instrum.* **51** 64
[12] Sheehan J and Hershkowitz N 2011 *Plasma Sources Sci. Technol.* **20** 063001
[13] Schweigert I V, Langendorf S J, Walker M L R and Keidar M 2015 *Plasma Sources Sci. Technol.* **24** 025012
[14] Ivanov V V, Popov A M and Rakhimova T V 1995 *Plasma Phys. Rep.* **21** 548
[15] Lagushenko R and Maya J 1984 *J. Appl. Phys.* **59** 3293
[16] Bugeat J P and Koppel C 1995 *23rd Int. Conf. on Electric Propulsion, IEPC 95-35*
[17] Schweigert I V and Keidar M 2017 *Plasma Sources Sci. Technol.* **26** 064001
[18] Schmidt N, Schulze J, Schungel E and Czarnetzki U 2013 *J. Phys. D: Appl. Phys.* **46** 505202